Vol. 21, e210008 (2024)
doi: 10.2142/biophysico.bppb-v21.0008

Biophysics and Physicobiology
https://www.jstage.jst.go.jp/browse/biophysico/

Regular Article

Resonance frequency measurement to identify stiffness variations based on photoacoustic imaging

Ananta Kusuma Yoga Pratama[1], Andreas Setiawan[2], Rini Widyaningrum[3], Mitrayana[1]

[1] *Department of Physics, Faculty of Mathematics and Natural Sciences, Universitas Gadjah Mada, Sleman, Yogyakarta 55281, Indonesia*
[2] *Department of Physics, Faculty of Sciences and Mathematics, Universitas Kristen Satya Wacana, Salatiga, Central Java 50711, Indonesia*
[3] *Department of Dentomaxillofacial Radiology, Faculty of Dentistry, Universitas Gadjah Mada, Sleman, Yogyakarta 55281, Indonesia*

Received August 10, 2023; Accepted January 15, 2024;
Released online in J-STAGE as advance publication January 20, 2024
Edited by Yasushi Sako

Linear assumption on the level of stiffness in a tissue shows a significant correlation with disease. Photoacoustic imaging techniques that are non-contact by design have been developed in this study to detect differences in phantom (soft tissue mimicking materials) stiffness. This study aims to detect differences in phantom stiffness based on the results of image reconstruction at the resonance frequency. Four phantom agars with differing concentrations were made to achieve different stiffnesses. The position of each phantom agar's highest photoacoustic signal amplitude is identified by a frequency modulation sweep. The characterization results show an increase in resonance frequency along with an increase in phantom stiffness. The image difference can be detected because the intensity of the photoacoustic image in samples that have a resonance frequency with laser modulation is comparatively higher than in other samples.

Key words: non-contact, laser, modulation, tissue, phantom

Significance

The present work aims to elucidate the significance of quantifying the photoacoustic resonance frequency in the identification of variations in stiffness inside biological specimens. The discovery holds significant implications for enhancing knowledge in the field of photoacoustic methodology for non-destructive and non-contact detection of variations in mechanical properties, particularly in biological or soft tissue samples. The photoacoustic approach holds potential for clinical applications due to its non-destructive and non-contact characteristics, which contribute to enhanced patient comfort during examination.

Introduction

Identification of soft tissue properties is one of the biological markers of a disease, besides using blood and urine media [1]. Changes in the mechanical properties of soft tissues are important parameters that are widely studied because pathological processes often change the structure of soft tissues and can result in mechanical properties changes [2].

Corresponding author: Mitrayana, Universitas Gadjah Mada, Sleman, Yogyakarta 55281, Indonesia. ORCID iD: https://orcid.org/0000-0002-2684-7950, e-mail: mitrayana@ugm.ac.id

Evaluation of soft tissue mechanical properties is relatively more complicated and challenging because their characteristics are often highly nonlinear and anisotropic. However, simple first-order linear assumptions of elastic and isotropic materials have often been applied as a simplification of tissue mechanical properties, where stiffness can be easily expressed using a simple modulus of elasticity [3].

Linear assumption of the level of stiffness in a tissue shows a significant correlation with disease. For example, in mechanical testing of breast tissue affected by cancer, there is an increase in the stiffness value to 16.2 kPa compared to normal tissue, which has a stiffness value of around 3.2 kPa [4]. Increased stiffness also occurs in tissues with cirrhosis of the liver and in several cases of other diseases. Thus, the difference in the level of stiffness in the tissue can reflect the pathological condition of the tissue, so it can be used as one of the parameters for tissue characterization that is useful for clinical applications in assisting the diagnosis of a disease.

Differences in the stiffness of elastic materials can easily be detected using mechanical tests by comparing the correlation between strength and strain. However, mechanical testing has the disadvantage of damaging the material, making it unsuitable for biological materials [5]. Contact mechanical testing also limit flexibility in clinical applications, e.g. wound surfaces, burns, abrasions, infections or patient discomfort [6]. To address this issue, imaging techniques that are non-destructive by design have been developed to detect changes in tissue stiffness. However, each imaging modality has limitations in certain aspects of its clinical application. For instance, in the case of cirrhosis of the liver, which significantly increases the stiffness of the liver tissue as a whole but still looks normal on ultrasound examination [7].

In this context, the photoacoustic (PA) technique can be an alternative imaging method for identifying differences in stiffness due to its working method, which combines optical and mechanical characteristics in its measurement. Despite its application, most PA imaging studies have only explored the optical absorption effect of the sample. The PA signal generation mechanism itself also involves interaction between the modulated laser and the sample, which produces mechanical vibrations on the sample surface [8]. The natural vibrational frequency of the sample will increase along with increasing stiffness, as has been proven in previous study [9]. In that research, a minisensor based on photoacoustic endoscopy (photoacoustic cell) was developed to characterize the amplitude of photoacoustic signals in silicone rubber samples that have different stiffness variations. The outcomes of the experiments indicate that the resonance frequency of the photoacoustic cell is higher with a higher Young's modulus value. These results also demonstrate the feasibility of the PA technique as a method of characterizing stiffness in soft tissues. However, the use of the photoacoustic cell will limit the dimensions of the sample, and the measurement is still contact based with sample. In addition, the experiment has not produced images of the samples tested, so they do not have spatial resolution.

This study aims to develop a non-contact measurement system based on photoacoustic techniques to detect differences in soft tissue phantom stiffness based on the results of image reconstruction at the resonance frequency. The photoacoustic signal is detected by the microphone as an air-coupled transducer, enabling non-contact measurements [10,11]. Phantom samples are objects designed to mimic the properties of biologic tissues, such as acoustic impedance, acoustic propagation velocity, and attenuation coefficient. Phantom samples are made from powdered agar, which is processed into a solid (gel). Agar is frequently employed in the fabrication of phantoms for photoacoustic imaging [12,13] due to its analogous acoustic characteristics to those of human tissue [14].The use of agar tissue phantoms as samples will provide flexibility in making repeatable variations in stiffness properties, which aim to support the characterization and optimization of photoacoustic imaging systems. Variations in agar concentration will produce different levels of stiffness in the phantom [15]. The phantom is modeled like a damped spring-mass oscillator in order to observe the relationship the link between stiffness and resonance frequency through scanning over a specified modulation frequency range yields the highest amplitude position, which is validated using a damped oscillator amplitude curve model. At the resonance frequency, the image results of the four phantoms are analyzed to detect image differences.

Materials and Methods

Theory

The generation of photoacoustic waves in the target sample occurs due to the absorption of optical energy from the modulated laser and the rapid rise in temperature, causing a thermoelastic expansion that produces acoustic waves. The photoacoustic effect resulting from sample surface vibration can be modeled by a mass-spring damped oscillator propelled by an external force. The physical system of the spring (Fig. 1(b)) is similar to the interaction between a modulated laser and a tissue (Fig. 1(a)).

The formulation of a soft tissue model as a point is absorption expressed as [16]

$$\frac{\partial^2}{\partial t^2}p(t) + a^2\frac{\xi + \frac{4}{3}\eta}{\rho}\frac{\partial}{\partial t}p(t). + a^2c^2p(t) = \Gamma\frac{\partial H(t)}{\partial t}, \quad (1)$$

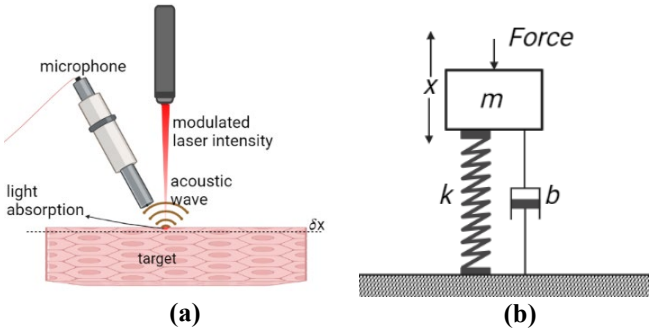

Figure 1 (a) Illustration of laser modulation generating a photoacoustic effect (b) Model of the damped mass - spring oscillator forcefully moved mass by force *F*.

where p is acoustic pressure, ρ is tissue density, a is constant of propagation phase constant, η is tissue shear viscosity, c is sound speed in tissue, ξ tissue bulk viscosity, and Γ is the Gruneisen parameter defined as $\Gamma = \beta c^2/C_p$, where C_p is specific heat capacity at constant pressure, and β is thermal expansion coefficient. The function $H(t)$ represents the heating effect resulting from the laser irradiation. Its magnitude is directly related to the product of the tissue's optical absorption coefficient and the optical fluence rate. The equation represented by Eq. (1) is a second order differential pressure equation that is influenced by the optical source term $\Gamma.\partial H(t)/\partial t$. To provide a clear understanding of the PA oscillation, we utilize a widely recognized damped mass-spring oscillator equation as a visual representation [17],

$$\frac{\partial^2}{\partial t^2}x(t) + \frac{b}{m}\frac{\partial}{\partial t}x(t) + \frac{k}{m}x(t) = \frac{F(t)}{m}, \tag{2}$$

where b is the damping coefficient, and k is the spring constant. Both equations exhibit strong agreement as second order differential equations. Hence, it is possible to establish a direct correspondence between the parameters : $1/m = \Gamma$, $b/m = a^2\left(\left(\xi + \frac{4}{3}\eta\right)/\rho\right)$, and $k/m = a^2c^2$. The analytical solution to Eq. (2) is obtained by simulating the PA signal generation of an elastic material through an externally stimulated impulse response using a modulated laser intensity. When laser excitation is in stress confinement, $F(t)$ can be approximated to zero and is comparable to impulse excitation. The driving force term is considered to be $F(t)/m = f_0 \cos \omega t$, and displacement of mass m is given by $x(t) = A\cos(\omega t - \theta)$, with

$$A = \frac{f_0}{\sqrt{\left(\frac{k}{m} - \omega^2\right)^2 + \left(\frac{b}{m}\omega\right)^2}}. \tag{3}$$

Largest displacement occurs at resonance frequency,

$$\omega_0 = \sqrt{\frac{k}{m} - \frac{1}{2}\left(\frac{b}{m}\right)^2}. \tag{4}$$

The stiffness of the material can be represented by a k value, which is proportional to $E.A/l$, where E is Young's modulus value, A is surface area and l is thickness of the sample [18]. The value of E affects the resonance frequency, so the higher the stiffness value, the higher the resonance frequency ($\omega \propto E$).

Preparation of Phantom Samples

Phantom samples were made from pure agar powder mixed in distilled water with a concentration of s_1=7.5 g/L; s_2=8 g/L; s_3=8.5 g/L, and s_4=9 g/L, to simulate biological tissues with different stiffness levels. The mixture of agar powder and water is stirred periodically while heated to 90 ºCelsius, then cooled in the mold to produce a homogeneous gel. Characterization studies of the phantom's Young's modulus with variations in agar concentration, obtained the relationship Young's modulus (in kilo Pascal (kPa)) = 0.349 $C^{1.87}$ (C is the concentration of agar in gram per liter) [19]. Using this relation, each phantom's Young's modulus is 15.12 kPa, 17.04 kPa, 19.1 kPa, and 21.25 kPa. The higher Young's modulus value, correlated with increased phantom stiffness [20]. To determine the performance of the

photoacoustic imaging system in detecting differences in stiffness, the targets were made into 3 mm thick slices, and arranged parallel as shown in Fig. 2.

Figure 2 Samples with varying agar concentration values s_1 to s_4 (low to high concentration), and similar cross sections.

Set Up a Photoacoustic Imaging System

The setup of the photoacoustic imaging experiment is shown in Fig. 3. For the light source, a focused 808 nm diode laser (JLM8050ZB-J2Y5 China) with a maximum power of 500 mW is used. The laser source is electronically modulated and controlled by the Arduino Nano microcontroller. The modulation of the diode laser was controlled by a transistor-transistor logic laser pin connected to a microcontroller using the pulse width modulation technique. The modulated beam is directed at the target, which triggers the emergence of photoacoustic waves. The photoacoustic signal is received by the sensor ECM8000 (Behringer–Germany) condenser microphone and sent to the computer via a sound card (UMC202HD Behringer–Germany). The microphone is installed at a distance of 10 mm from the object, forming an angle of 60° to the surface of the sample. The laser source and microphone are moved in the x-y direction by a stepper motor, which is also controlled by the Arduino Nano microcontroller.

The four phantom slices that has been prepared is placed on the sample table and scanned from point to point. The recorded photoacoustic signal is processed at each point and displayed using the LabVIEW program. To set the step resolution in the sample scanning process, enter the value of the stepper motor's number of steps, and measure the length of the shift in the x and y directions to determine the distance for each step.

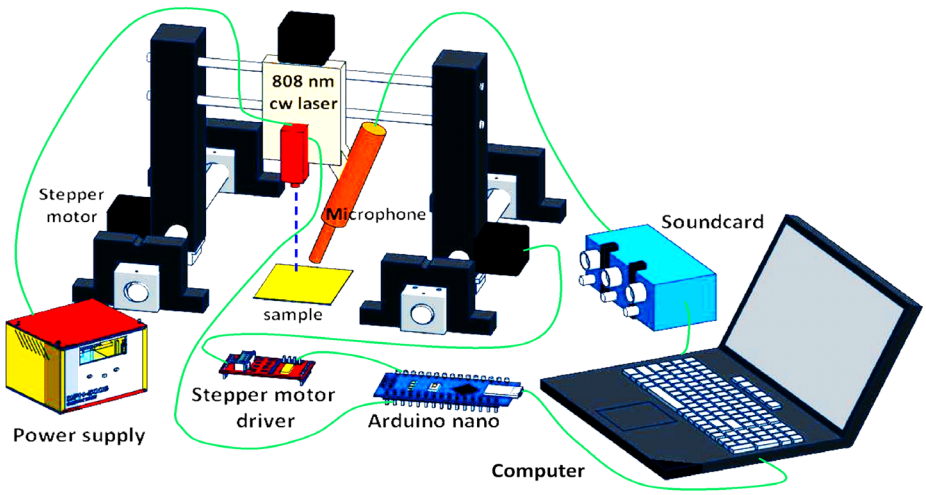

Figure 3 Experimental schematic diagram for a photoacoustic imaging system.

Phantom Stiffness Difference Detection

The measurement of the photoacoustic signal for each variation of the phantom sample has its maximum value when the

modulation frequency is close to the natural frequency, which is known as the resonance frequency. To determine the range of scanning frequencies, noise measurements are carried out up to a frequency limit of 20 kHz to determine the noise stability area. The resonance frequency is found by modulating the laser frequency for each sample of the stiffness variation and measuring the highest peak amplitude of the photoacoustic signal. Image reconstruction is carried out by scanning four phantom slices (Fig. 2) in parallel, using a modulation frequency diode laser according to the measured resonance frequency. The resulting image is analyzed to determine the effect of the resonance frequencies on the resulting image.

Results

Step resolution calibration is conducted on the stepper motor to ensure that no sample areas are double scanned or missed during the laser scanning procedure. For stepper motor calibration on the *x* and *y* axes, 20 steps are input for each, and the shift value is measured for every 5 steps. The results of the measurement of the shift length on the x-axis and y-axis optimum at value of 0.2 mm. To obtain a stable measurement of a photoacoustic signal, noise measurements of the environment and the system are collected in the range of the laser modulation frequency that will be used when the laser is turned off.

Noise measurements are carried out by measuring the response of sound signals from the environment and the system received by the microphone over a range of frequency variations. The measurements were conducted within a laboratory setting characterised by a relatively low ambient noise level and a considerable distance from any large gatherings of individuals. When the acoustic frequency filter within the system is adjusted to align with the laser modulation frequency, it effectively prevents the entry of external sounds with frequencies that do not correspond to the system into the microphone. These external sounds typically exhibit a normal sound intensity range of 25-30 dB within the room. From the results of measurements carried out three times on different days as shown in Fig. 4, for the frequency range 6.5 to 20 kHz, the system shows that the normalized noise signal response tends to be flat with a variation range between 0 to 0.11. The noise value exhibits a significant increase by one order of magnitude below this frequency. Consequently, the amplitude of the PA becomes challenging to discern from its surroundings because it is buried in the noise.

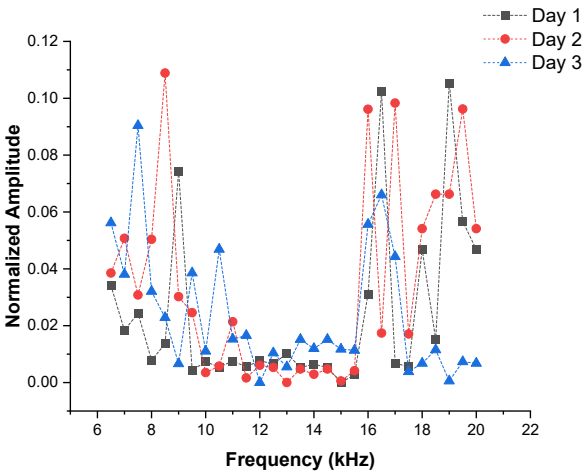

Figure 4 Noise intensity measurement from the environment and system.

The amplitudes of the PA signal in proportion to the modulation frequency were measured for the four samples of the phantom agar slices. Each measurement was repeated three times for each sample, and the average amplitude values are presented in Fig. 5. The PA signal in each sample is measured in the modulation frequency range between 13 and 19 kHz, with steps of 1 kHz. At each frequency point, the peak-to-peak amplitude of the PA signal is recorded to construct the photoacoustic signal spectrum. The Fourier transform was used to analyze signal modulation, and the resulting spectra included the square wave signals' basic frequencies as well as nearby frequencies. This is due to the fact that none of the square waves signals were exactly square. The photoacoustic interactions caused responses that expanded the photoacoustic frequency spectrum and increased the standard deviation for each frequency [21]. A curve fitting model is created based on the amplitude equation of the damped oscillations [22] as a method for locating the resonance frequency of each sample as shown in Fig. 5.

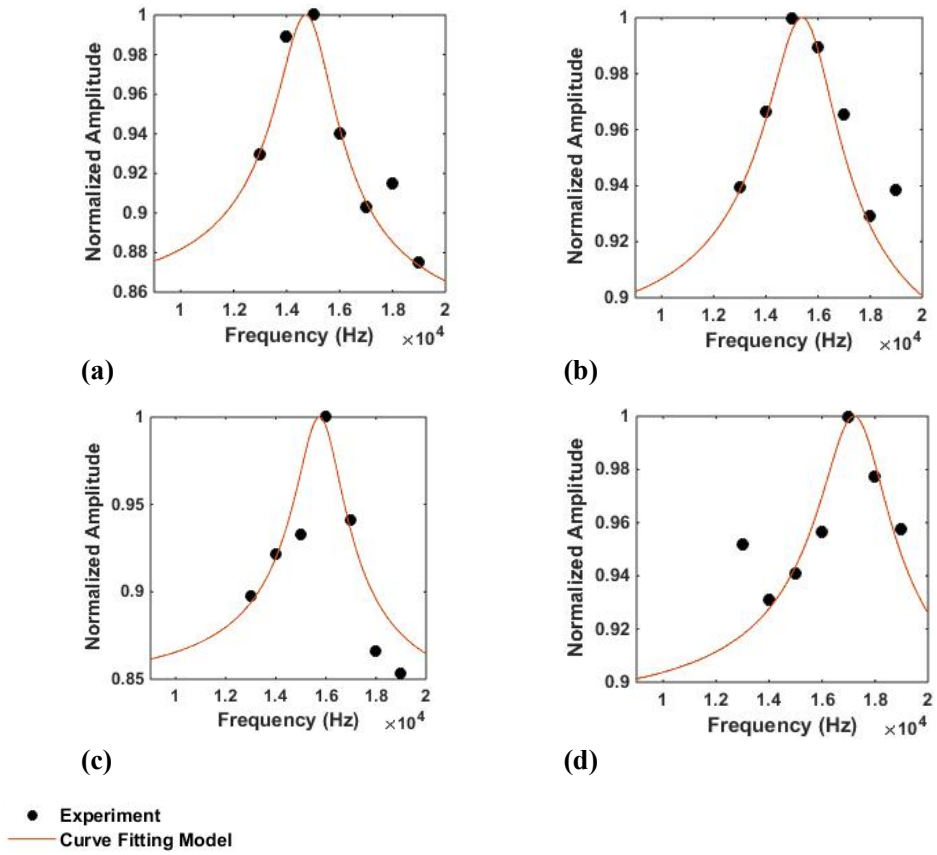

Figure 5 PA signal amplitude measured (N=3) as a function of modulation frequency for phantom with concentrations of (a) 7.5 g/L, (b) 8 g/L, (c) 8.5 g/L, (d) 9 g/L.

Resonance frequency position selection can be determined based on the highest signal amplitude value when given a variation of the modulation frequency. Based on the measured signal waveforms depicted in Figs. 5(a)-5(d), the resonance frequencies' averages and standard deviations for the agar concentrations of 7.5 g/L, 8 g/L, 8.5 g/L, and 9 g/L are as follows: 14.6 ± 0.2 kHz, 15.4 ± 0.1 kHz, 15.9 ± 0.1 kHz, and 17.2 ± 0.2 kHz, respectively. The resulting resonance frequency values allow one to establish a correlation between the measured frequency and the stiffness level of each sample, as shown in Fig. 6. Phantom with higher Young's modulus mean higher stiffness, exhibit higher resonance frequencies, which match the predictions from Eq. (3).

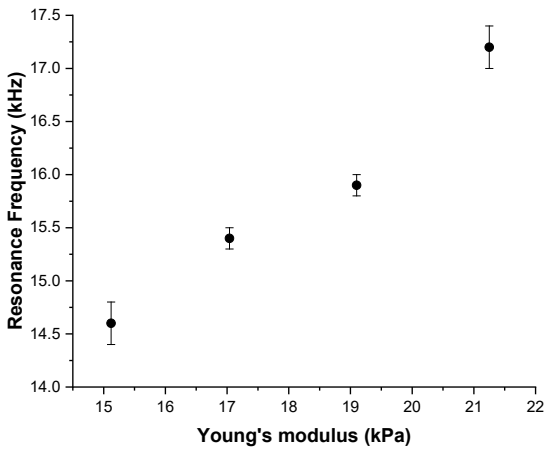

Figure 6 The value of the phantom resonance frequency for four different agar phantom samples (N=3).

Four phantom slices with small areas (1.1 cm×0.3 cm) that have different concentrations are positioned parallel to one another in the sequence s_1, s_2, s_3, and s_4 in order to test the efficiency of the photoacoustic system in imaging phantoms with various degrees of stiffness. The photoacoustic signal is scanned at each point (pixel) throughout the full surface area as part of the image reconstruction process. Fig. 7(a) displays the image results photoacoustic imaging system with a laser modulation frequency of 14.6 kHz, and Fig. 7(b) displays the same results with a laser modulation frequency of 15.4 kHz.

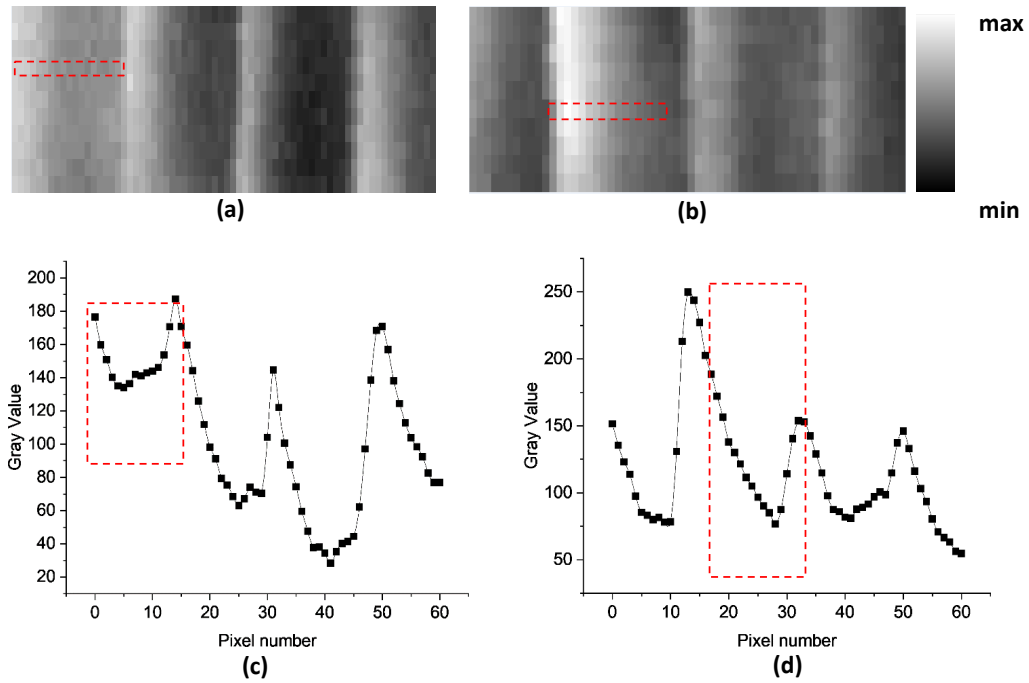

Figure 7 Photoacoustic images of four phantoms s_1, s_2, s_3, and s_4 at a modulation frequency of (a) 14.6 kHz, (b) 15.4 kHz. Pixel plot profile on image cross section at a modulation frequency of (c) 14.6 kHz. (d) of 15.4 kHz.

Fig. 7(a) shows there is a variation in the visual contrast of the resulting image. High PA signal exhibited more lighter color than low PA signal. The image of phantom s_1 is dominated by the color light gray, whereas the images of phantoms s_2, s_3, and s_4 are dominated by the darker color (black). The pixel profile plot in Fig. 7(c) of the region of interest phantom s_1 (red box) reveals the gray value of the phantom s_1 is substantially greater than the other phantom samples. This indicates that phantoms with an agar concentration of 7.5 g/L generate a higher PA signal at a modulation frequency of 14.6 kHz. Fig. 7(b) demonstrates that the phantom s_2 image contains a greater proportion of light gray than the other phantom, indicating a stronger PA signal. According to the ROI pixel profile plot in Fig. 7(d), phantom s_2 has a significantly different gray value than the other phantoms. This means that phantoms with an 8.0 g/L concentration generates a stronger PA signal for a 15.4 kHz modulation frequency.

Discussion

In this study, a photoacoustic technique with a continuous laser as an irradiation source was applied to image samples with different stiffness levels. Measurements of photoacoustic signals on samples with varying Young's modulus values revealed variances in the obtained signal patterns in earlier investigations [9,23]. The use of photoacoustic cells and ultrasonic transducers adopts the concept of a contact measurement design, thus limiting the possibilities for clinical and pre-clinical applications. Therefore, a photoacoustic imaging system was developed using a more flexible open configuration with an air-coupled transducer in the form of a condenser microphone. From our previous work, the oral soft tissue was imaged by setting the laser modulation frequency to 17.8 kHz [24]. The use of modulation frequencies at 19 kHz has been reported to be capable of producing image contrast in periodontal tissue to distinguish between healthy and periodontitis tissue as shown in Fig. 8 [25]. These results show that variations in the modulation frequency over the audiosonic range can be applied to soft tissue characterization. However, the PA resonance effect generated by the mechanical resonance properties of the specimen has not been investigated further, with just changes in surface color evaluated.

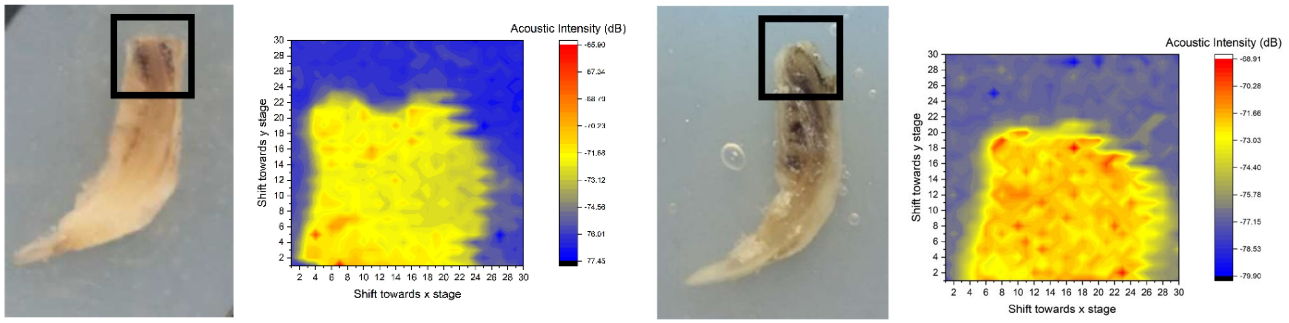

(a) **(b)**

Figure 8 Incisors specimens of Sprague Dawley rat's periodontal tissue and photoacoustic images: (a) health tissue (b) periodontitis tissue. The figure is used with permission from the authors [25].

Utilization of a continuous laser source modulated in the audiosonic range is necessary to produce a photoacoustic signal capable of being detected by a microphone [21,26,27]. The use of modulation frequency in the area below 20 kHz brings benefits, including better efficiency of acoustic transmission in the air, so that measurements can be made non-contact using a condenser microphone. However, using an audiosonic transducer in an open configuration is vulnerable to external (environmental) noise. In anticipation of this, the implementation of a higher laser modulation frequency (> 10 kHz) is relatively more stable in suppressing environmental noise fluctuations. Fig. 4 shows that the modulation frequency above 10 kHz has a minimum and flat noise level. The modulation frequency area with a flat noise response is used as the modulation frequency variation area in searching for the highest photoacoustic signal amplitude.

Periodic heating by the modulated laser induces mechanical vibrations on the sample's surface, which leads to thermal expansion and the generation of acoustic waves. The relationship between the initial pressure increase and thermal expansion shows that the photoacoustic source is a strain source [28]. This means that variations in Young's modulus values (stiffness level) characterize the strength of the strain pulse or PA source.

Sweeping frequency modulation at phantom agar samples with different stiffness will produce different resonance frequencies that provide a contrast perspective apart from optical absorption. Fig. 5 shows that each concentration of agar shows a peak amplitude at a different modulation frequency. Variation of concentration to be selected close to the value of stiffness in breast cancer (9–17 kPa) [29]. By using the curve fitting model for the recorded waveform, the resonance frequencies for each sample (s_1, s_2, s_3, and s_4) are plotted in the graph shown in Fig. 6. It appears that the phantom with a higher degree of stiffness has a higher resonance frequency, as predicted by Eq. (4).

The photoacoustic image demonstrates that when the laser modulation frequency is close to or equal to the phantom's resonance frequency, the image contrast is predominantly brighter compared to other phantoms, which are darker in color (black) because the resonance frequency is positioned relatively far away. The scanning process for image reconstruction is carried out with a size of 60 x 10 pixels, resulting in a total of 600 measurement points. The average shift of the x-y stage step for each pixel is 0.2 mm. For each measurement point, the photoacoustic signal is recorded, and its amplitude is calculated using the Fourier transform. This peak value is subsequently recorded as intensity level data on a single pixel, which is then converted into 256 gray-level values. This is repeated at every surface measurement point in order to generate a two-dimensional photoacoustic image.

The plot profile, under ideal circumstances of a homogenous sample, should have a uniform shape across the whole surface [30]. Variations in measurements may be caused by nonuniform light fluence on the surface [31], and surface roughness of the sample [32]. The boundary line of the phantom intersection experiences repetitive reflection toward a very thin slit, which results in an increase in absorption as a result of repeated laser-material interactions [33] and shows up as an increase in the gray value of the pixel plot profile (Fig 7(c), and 7(d)). However, the photoacoustic technique still presents the difference in mechanical resonance for the different phantom stiffnesses tested. This research is still limited to phantom studies, and further research is needed to verify the performance of photoacoustic imaging for ex vivo tissue stiffness, due to the complexity of heterogeneous tissue properties.

Conclusion

This study proposes non-contact photoacoustic imaging to detect differences in phatom stiffness based on frequency resonance measurements. The measurement results show that there is a relationship between the increase in stiffness and the positional resonance frequency. Image reconstruction shows that the contrast of the PA phantom image at the resonance frequency position is relatively brighter compared to other phantoms, which are darker in color, so that differences in stiffness can be detected.

Conflict of Interest

Authors have no conflict of interest to declare.

Author Contributions

Ananta Kusuma Yoga Pratama: data collection, formal analysis, writing-original draft preparation. Andreas Setiawan: conceptualization, result validation, reviewing and editing. Rini Widyaningrum: reviewing. Mitrayana: supervision, result validation, reviewing.

All authors discussed the result and commented on the manuscript.

Data Availability

The evidence data generated and/or analyzed during the current study are available from the corresponding author on reasonable request.

Acknowledgements

This study was supported by The Indonesian Endowment Fund for Education/ Lembaga Pengelola Dana Pendidikan (LPDP) and Center for Higher Education Funding/ Balai Pembiayaan Pendidikan Tinggi (BPPT).

References

[1] Vasan, R. S. Biomarkers of cardiovascular disease: Molecular basis and practical considerations. Circulation 113, 2335–2362 (2006). https://doi.org/10.1161/CIRCULATIONAHA.104.482570

[2] Kmiecik, B., Skotny, A., Detyna, J. Structure and mechanical properties of soft tissues during selected pathological processes. J. Blood Disord. Transfus. 5, 1–5 (2017). https://doi.org/10.4172/2327-5146.1000285

[3] Al Mayah, A. Biomechanics of soft tissues, principles and applications. (CRC Press, New York, 2018).

[4] Shiina, T., Nightingale, K. R., Palmeri, M. L., Hall, T. J., Bamber, C. J., Barr, R. G., et al. WFUMB guidelines and recommendations for clinical use of ultrasound elastography: Part 1: Basic principles and terminology. Ultrasound Med. Biol. 41, 1126–1147 (2015). https://doi.org/10.1016/j.ultrasmedbio.2015.03.009

[5] Biswas, D., Vasudevan, S., Chen, G. C. K., Sharma, N. Quantitative photoacoustic characterization of blood clot in blood: A mechanobiological assessment through spectral information. Rev. Sci. Instrum. 88, 024301 (2017). https://doi.org/10.1063/1.4974954

[6] Hosseinaee, Z. Towards non-contact photoacoustic imaging [review]. Photoacoustics 20, 100207 (2020). https://doi.org/10.1016/j.pacs.2020.100207

[7] Ophir, J. A review of theoretical and experimental aspects of imaging the elastic attributes of tissue in vivo. Res. Dev. Breast Ultrasound 3–6 (2006). https://doi.org/10.1007/4-431-27008-6_2

[8] McDonald, F. A., Wetsel, G. C. Generalized theory of the photoacoustic effect. J. Appl. Phys. 49, 2313–2322 (1978). https://doi.org/10.1063/1.325116

[9] Wadamori, N. Non-restrained measurement of Young's modulus for soft tissue using a photoacoustic technique. Appl. Phys. Lett. 105, 103707 (2014). https://doi.org/10.1063/1.4893725

[10] Setiawan, A., Setiaji, F. D., Dewantoro, G., Wibowo, N. A. Photoacoustic tomography system for roughly painted micro objects. J. Electromagn. Eng. Sci. 19, 197–203 (2019). https://doi.org/10.26866/jees.2019.19.3.197

[11] Tasmara, F. A., Widyaningrum, R., Setiawan, A., Mitrayana, M. Photoacoustic imaging of hidden dental caries using visible–light diode laser. J. Appl. Clin. Med. Phys. 24, e13935 (2023). https://doi.org/10.1002/acm2.13935

[12] Gehrung, M., Bohndiek, S. E., Brunker, J. Development of a blood oxygenation phantom for photoacoustic tomography combined with online pO2 detection and flow spectrometry. J. Biomed. Opt. 24, 121908 (2019). https://doi.org/10.1117/1.jbo.24.12.121908

[13] Avigo, C., Lascio, N. D., Armanetti, P., Kusmic, C., Cavigli, L., Ratto, F., et al. Organosilicon phantom for photoacoustic imaging. J. Biomed. Opt. 20, 046008 (2015). https://doi.org/10.1117/1.jbo.20.4.046008

[14] Manickam, K., Machireddy, R. R., Seshadri, S. Characterization of biomechanical properties of agar based tissue mimicking phantoms for ultrasound stiffness imaging techniques. J. Mech. Behav. Biomed. Mater. 35, 132–143 (2014). https://doi.org/10.1016/j.jmbbm.2014.03.017

[15] Li, C., Huang, Z., Wang, R. K. Elastic properties of soft tissue-mimicking phantoms assessed by combined use of laser ultrasonics and low coherence interferometry. Opt. Express 19, 10153–10163 (2011). https://doi.org/10.1364/OE.19.010153

[16] Gao, F., Feng, X., Zheng, Y. Photoacoustic elastic oscillation and characterization. Opt. Express 23, 20617–20628 (2015). https://doi.org/10.1364/oe.23.020617
[17] Chow, T. L. Classical mechanics, 2nd ed. (CRC Press, New York, 2013).
[18] Inman, D. J. Engineering vibrations, 3rd ed. (Pearson Education, Inc., New Jersey, 2008).
[19] Hall, T. J., Bilgen, M., Insana, M. F., Krouskop, T. A. Phantom materials for elastography. IEEE Trans. Ultrason. Ferroelectr. Freq. Control. 44, 1355–1365 (1997). https://doi.org/10.1109/58.656639
[20] Askeland, D. R., Wright, W. J. The science and engineering of materials, 7th ed. (Cengage Learning, Boston, 2016).
[21] Setiawan, A., Rondonuwu, F. S., Setiaji, F. D. Analyzing the shape of photoacoustic signal on audible frequency modulation. J. Phys. Conf. Ser. 1307, 012017 (2019). https://doi.org/10.1088/1742-6596/1307/1/012017
[22] Deshmukh, P. C. Foundations of classical mechanics (Cambridge University Press, United Kingdom, 2019).
[23] Singh, M. S., Jiang, H. Ultrasound (US) transducer of higher operating frequency detects photoacoustic (PA) signals due to the contrast in elastic property. AIP Adv. 6, 025210 (2016). https://doi.org/10.1063/1.4942106
[24] Widyaningrum, R., Agustina, D., Mudjosemedi, M., Mitrayana. Photoacoustic for oral soft tissue imaging based on intensity modulated continuous-wave diode laser. Int. J. Adv. Sci. Eng. Inf. Technol. 8, 622–627 (2018). https://doi.org/10.18517/ijaseit.8.2.2383
[25] Sari, A. W., Widyaningrum, R., Mitrayana, M. Photoacoustic imaging for periodontal disease examination. J. Lasers Med. Sci. 13, e37 (2022). https://doi.org/10.34172/jlms.2022.37
[26] Miklos, A., Hess, P. Modulated and pulsed photoacoustics in trace gas analysis. Anal. Chem. 72, 30A–37A (2000).
[27] Widyaningrum, R., Mitrayana, M., Gracea, R. S., Agustina, D., Mudjosemedi, M., Silalahi, H. M. The influence of diode laser intensity modulation. J. Lasers Med. Sci. 11, S92–S100 (2020). https://doi.org/10.34172/jlms.2020.S15
[28] Singh, M. S., Jiang, H. Elastic property attributes to photoacoustic signals: an experimental phantom study. Opt. Lett. 39, 3970–3973 (2014). https://doi.org/10.1364/ol.39.003970
[29] Samani, A., Zubovits, J., Plewes, D. Elastic moduli of normal and pathological human breast tissues: An inversion-technique-based investigation of 169 samples. Phys. Med. Biol. 52, 1565 (2007). https://doi.org/10.1088/0031-9155/52/6/002
[30] Schoonover, R. W., Anastasio, M. A. Image reconstruction in photoacoustic tomography involving layered acoustic media. J. Opt. Soc. Am. A Opt. Image Sci. Vis. 28, 1114–1121 (2011). https://doi.org/10.1364/JOSAA.28.001114
[31] Bu, S., Liu, Z., Shiina, T., Kondo, K., Yamakawa, M., Fukutani, K., et al. Model-based reconstruction integrated with fluence compensation for photoacoustic tomography. IEEE Trans. Biomed. Eng. 59, 1354–1363 (2012). https://doi.org/10.1109/TBME.2012.2187649
[32] Verrina, V., Edward, S., Zhang, H., Antoncecchi, A., Witte, S., Planken, P. Role of scattering by surface roughness in the photoacoustic detection of hidden micro-structures. Appl. Opt. 59, 9499–9509 (2020). https://doi.org/10.1364/ao.397264
[33] Setiawan, A., Suparta, G. B., Mitrayana, Nugroho, W. Surface crack detection with low-cost photoacoustic imaging system. Int. J. Technol. 9, 159–169 (2018). https://doi.org/10.14716/ijtech.v9i1.1506